

Structural and Physical Properties Study of Some Provkite Samples Used as Cathodes in Solid Oxide Fuel Cells

I.M. Ashraf, Ibraheem Othman Ali¹, A.G. Mostafa² and M.G. Ismaeil *

Phys. Dept., Faculty of Science, Aswan Univ., Aswan, Egypt.

¹. Chem. Dept., Faculty of Science, Al-Azhar Univ., Nasr City (11884), Cairo, Egypt.

². Phys. Dept., Faculty of Science, Al-Azhar Univ., Nasr City (11884), Cairo, Egypt.

*elomdaa_76@yahoo.com

Abstract: Some lanthanum strontium cobalt iron perovskites have been prepared by the sol-gel method. Characterization by several techniques (XRD, TGA/DTA, TEM, UV-VIS, VSM and Dc electrical conductivity) have been performed. From XRD data, a distorted rhombohedral perovskite structure has been confirmed for all samples. Both XRD calculations and TEM images show that all crystallites are in the nano-size. From the electrical conductivity measurements, it can be stated that all the studied samples behave like semiconductors. The magnetic saturation and remnant magnetization decreased with increasing lanthanum content. The continuous loss of lattice oxygen upon heating leads to the increase of oxygen vacancies and the thermal reduction of the transition metal cations tends to be easier with the increase of La doping. Both the electrical and the optical band gap energies decreased as La oxide content was increased.

[Ashraf IM, Ali IO, Mostafa AG and Ismaeil MG. **Structural and Physical Properties Study of Some Provkite Samples Used as Cathodes in Solid Oxide Fuel Cells.** *Nat Sci* 2017;15(10):101-107]. ISSN 1545-0740 (print); ISSN 2375-7167 (online). <http://www.sciencepub.net/nature>. 14. doi:[10.7537/marsnsj151017.14](https://doi.org/10.7537/marsnsj151017.14).

Keywords: Perovskites, Semiconductor materials, oxygen vacancies, thermal reduction.

1. Introduction

Perovskite, type transition metal oxides with the general formula ABO_3 , have been subjected to intensive scientific investigation since the discovery of magnetoresistance in manganese based compounds [1,2]. A variant perovskite structure having the formula $(A_2B'B''O_6)$, is also prepared and named double perovskite (DP) which presents interesting physical phenomena.

Lanthanum-Strontium-Cobalt-Iron (LSCF) perovskites seem to be particularly interesting in terms of their possible applications. These materials have been extensively studied as potential cathode materials [3-5]. Solid Oxide Fuel Cells (SOFC) operating in an intermediate temperature range (600-800°C) are expected to overcome major problems, which hinder commercialization of SOFC technology. A lower operating temperature, however, requires higher activity of electrodes, especially high ionic conductivity of electrolyte, low over potential and low overall internal resistance loss. These requirements can be met by developing new electrode materials, new cell assembly concepts and novel fabrication methods [6-12]. For cathode materials, the occurrence of mixed ionic-electronic conductivity can be highly beneficial, since it allows the oxygen reduction along the entire surface of the cathode material. Oxygen ions can transport in the whole cathode bulk [13], but it requires an existence of the oxygen non-stoichiometry in the cathode material during the temperature range of working. Among the possible

candidates for SOFC cathodes, LSCF oxide systems are interesting because of their high mixed ionic-electronic conductivities. LSCF compounds with higher strontium content exhibit higher oxygen nonstoichiometry appeared at relatively lower temperatures [14].

However $(La_{1-x}Sr_xFeO_{3-\delta})$ perovskite system has been extensively studied in aspects of defect chemistry [15-19], charge transport property [17, 19-22], oxygen permeation property [19, 23-24] and chemical compatibility [25-26]. However, very few studies have been published on ferrite-based perovskites with other A-site cations [27-30]. Kharton et al. [17] studied the oxygen non-stoichiometry, mixed conductivity and surface exchange-related processes of $Ln_{0.5}M_{0.5}FeO_{3-\delta}$ ($Ln=La, Pr, Nd, Sm, M=Sr, Ba$) perovskites in order to be used as cathodes in SOFC. Piao et al. [31] studied the crystal structure, thermal expansion, electrical conductivity and electrochemical performance of $Pr_{1-x}Sr_xFeO_{3-\delta}$ as potential cathode materials for SOFC. Such $Pr_{1-x}Sr_xFeO_{3-\delta}$ cathodes were shown to be superior in performance over the traditional $La_{0.8}Sr_{0.2}MnO_3$ cathode. Ecija et al. [32] studied the influence of the average ionic radius of the A-site cation on the structural, morphological and electrical properties of $Ln_{0.5}M_{0.5}FeO_{3-\delta}$ ($Ln=La, Nd, Sm; M=Ba, Sr$). They try to combine different Ln^{3+} and M^{2+} ions to tune the average ionic radius of the A-site cation while keeping the doping level in A position constant and A-site cation size disorder. Their results suggested that the

sample with the higher average ionic radius showed the highest value of conductivity.

However, in the present paper, the synthesis of $\text{La}_{1-x}\text{Sr}_x\text{Co}_{0.7}\text{Fe}_{0.3}\text{O}_3$ ($0.4 \leq x \leq 0.7$) nano-crystallites by sol-gel method has been reported. The main focus is to investigate the effect of the gradual replacing of Sr by La ions on the structure, dc conductivity (σ_{dc}), magnetic and optical properties of the studied samples.

2. Experimental

2.1. Sample Preparation

The metal nitrates were weighed according to the desired amount to form a solution in bi-distilled water. Such solution was mixed and stirred on a hot plate at 150 °C until a gel was formed. The obtained gel was heated further until solid foam was obtained. This foam was then ground and dried at 200 °C overnight. Then the obtained dried resin was powdered in an agate mortar and then pressed at 300 MPa using a 13 mm cylindrical die. The composition and nomination of the obtained solid samples are exhibited in Table (1).

Table 1. The compositions of the prepared samples

number	Chemical composition	nomination
1	$\text{La}_{0.4}\text{Sr}_{0.6}\text{Co}_{0.7}\text{Fe}_{0.3}\text{O}_3$	LSCF 4673
2	$\text{La}_{0.5}\text{Sr}_{0.5}\text{Co}_{0.7}\text{Fe}_{0.3}\text{O}_3$	LSCF 5573
3	$\text{La}_{0.6}\text{Sr}_{0.4}\text{Co}_{0.7}\text{Fe}_{0.3}\text{O}_3$	LSCF 6473
4	$\text{La}_{0.7}\text{Sr}_{0.3}\text{Co}_{0.7}\text{Fe}_{0.3}\text{O}_3$	LSCF 7373

2.2. TGA/DTA Analysis

The dried powdered gel was subjected to thermo-gravimetric and differential thermal analysis (TG/DTA) technique, using NETZSCH STA 449F3 apparatus, in order to determine the suitable sintering temperature.

2.3. X-Ray Diffraction Analysis

X-ray diffraction (XRD) patterns were collected by using a Bruker D8 Advance X-ray powder diffractometer (40 kV, 50 mA, sealed Cu X-ray tube, $\lambda = 1.5406 \text{ \AA}$).

2.4. TEM Analysis

Morphology and crystal structure of the studied perovskites along with selected area electron diffraction (SAED) patterns were examined by applying transmission electron microscopy (TEM) using, JEOL JEM 2100 HRTEM, outfitted with oxford energy dispersive x-ray spectroscopy detector at an acceleration voltage of 200 kV.

2.5. DC Electrical Measurements

The temperature dependence dc electrical conductivity (σ_{dc}) of the sintered samples was measured by applying the two probe technique at temperatures between RT and 600 °C in air. Silver wires and silver paste were used as contacts and the

measurements were carried out by using Agilent 4284A LCR Meter Bridge.

2.6. Magnetic Measurements

Magnetic characterization was carried out by using a vibrating sample magnetometer (VSM) (Lake Shore with a sensitivity of 1×10^{-6} emu). Hysteresis measurements were made with a field oscillating between $\pm 20,000$ Gauss.

2.7. Optical Measurements

An ultraviolet-visible (UV-VIS) diffuse reflectance spectrometer (PG Instruments, UK) was used to obtain the optical transmission spectra.

Detailed experimental information about the method of preparation, calcination and experimental measurements are found in Ref. [33].

3. Results and Discussion

3.1. Thermal Analysis

The obtained TGA/DTA curve for the sample ($\text{La}_{0.5}\text{Sr}_{0.5}\text{Co}_{0.7}\text{Fe}_{0.3}\text{O}_3$) can be seen in Fig. (1) as representative curve, and all samples show approximately similar behavior. It is found that the total weight loss occurred in three main stages. The first stage may be due to the presence of some moisture content through the nano-crystallites. The weight loss in the second stage can be attributed mainly to the decomposition of polyvinyl alcohol (PVA) used during synthesis. The third stage may be due to the conversion of the metal hydroxides to the corresponding metal oxides. The calcination temperature was determined from TGA/DTA curves and was identified to be 930 °C. Similar behavior has been reported for other perovskite phase formation at very high temperature [34]. Based on these results all samples were calcined at 1000°C for 24 h.

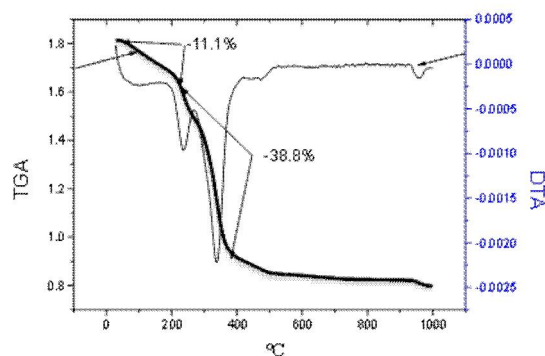


Figure 1. TGA/DTA curves for LSCF 5573 perovskite, as representative curve

3.2. XRD Analysis

Fig. (2) shows the obtained XRD patterns of all the studied perovskite samples. The XRD results reveal that the main crystal structure is a rhombohedral perovskite phase for all samples. The

appeared main diffraction peaks in these spectra confirm the formation of a single rhombohedral perovskite phase. There appeared also some slight peaks of very small intensities indicated the presence of very slight amount of unreacted oxides as impurities. Such very little impurities cannot be completely identified. However, it can be stated that, all the studied samples reveal a single phase with rhombohedral distorted perovskite structure. No reflection peaks of iron oxide were observed by XRD suggesting the incorporation of all iron into the perovskite phase. There present a very small amount of Co_3O_4 , where the response of this crystalline phase is also very low. These very little impurities appeared approximately of no effect on the obtained main perovskite phase [35]. From the obtained XRD patterns, the unit cell parameters, crystal size and cell volume are calculated and the obtained values are listed in Table (2).

Table 2. Cell parameters (a, b and c), cell volume and crystallite size of the studied perovskites

Sample Nomination	a = b a (Å°)	c (Å°)	Unit cell volume (nm ³)	Crystal size
LSCF 4673	5.3571	13.1863	0.3784	25.6
LSCF 5573	5.3955	13.2356	0.3853	27.4
LSCF 6473	5.4682	13.2556	0.3964	28.8
LSCF 7373	5.5236	13.2854	0.4053	31.7

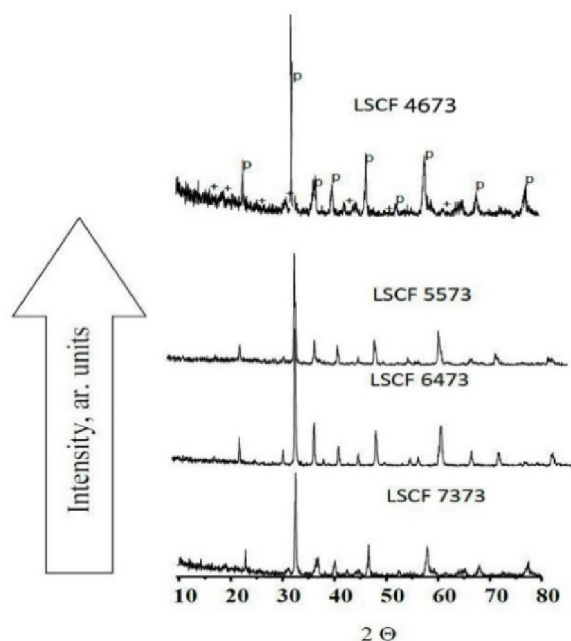


Figure 2. XRD patterns of all samples

The slight gradual increase of both the unit cell volume and crystallite size with increasing La content are presented graphically in Figs. (3 & 4) respectively. Such increase may be due to the substitution of Sr^{2+} by

La^{3+} cations, where the ionic radius of La^{3+} (1.36 Å°) is slightly lower than that of Sr^{2+} (1.44 Å°).

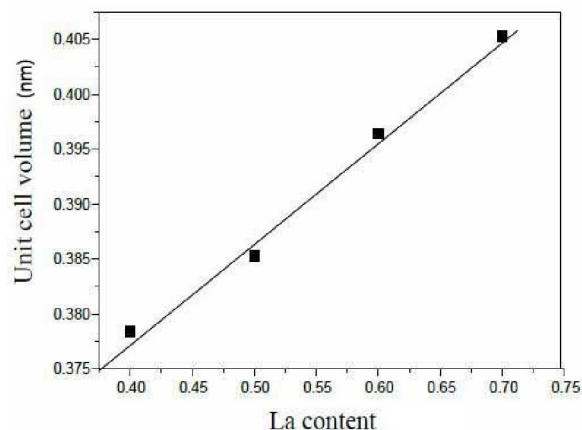


Figure 3. The change of the unit cell volume with La content

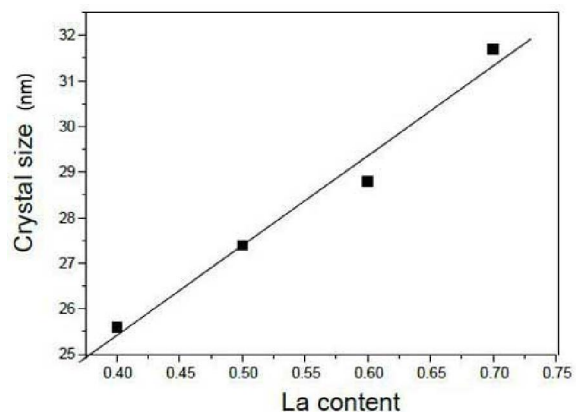


Figure 4. The change of the crystallite size with La content

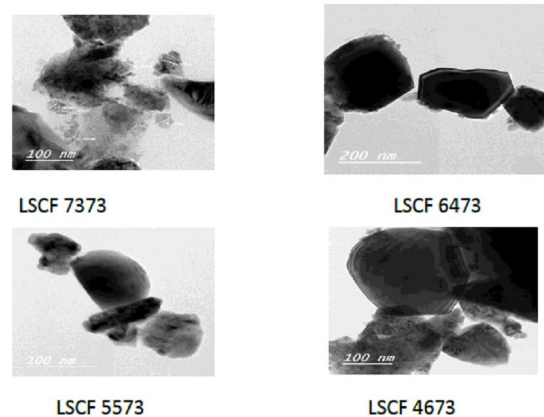


Figure 5. TEM micrographs of all samples

3.3. TEM Studies

The actual size of particles was determined by treating the sample in ultrasound bath and further

characterized by electron microscope in transmission mode. The obtained transmission electron micrographs are given in Fig. (5), where they show that all particles are nano-sized, spheroids and ellipsoids.

3.4. DC Electrical Conductivity

Electrical conductivity of a material can proceed either by electrons and/or ions. In perovskite oxides, owing to the co-presence of transition metal ions and oxygen vacancies, both types of conduction are present. But ionic conductivity is much lower than the electronic conductivity. Therefore, it can be assumed reasonably that the electronic conductivity is predominant [36]. Therefore, the variation of the electrical conductivity with temperature for the studied perovskite samples can be shown in Fig. (6). It can be seen that, the conductivity increased with temperature, as expected for semiconductors. This behavior is consistent with the small polaron conduction mechanism [14, 37].

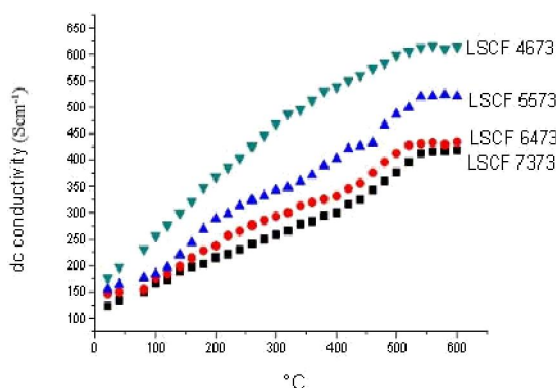


Figure 6. DC electrical conductivity (σ_{dc}) (Scm^{-1}) of all samples

It appeared that the conductivity increased with increasing temperature up to about 520 °C and then it shows a stable value up to 600 °C. The general trend and the observed behavior are similar to those reported in literature [37-39]. However, in LSCF materials, the conductivity is controlled by small polaron hopping mechanism, with charge transfer being thermally activated from RT and up to about 520 °C. According to Arrhenius equation,

$$\sigma_T = \sigma_0 \exp\left(\frac{\Delta E}{k_B T}\right)$$

where, σ_T is the temperature dependent conductivity, σ_0 is the pre-exponential factor, ΔE is the activation energy, T is the absolute temperature and k_B is Boltzmann constant. The activation energies can be then calculated and the calculated electrical activation energies of the studied perovskites are exhibited in Table (3), where it is seen that ΔE increases gradually with increasing La content.

Table 3. The variation of the activation energy (ΔE) with La content

La content	0.4	0.5	0.6	0.7
ΔE	3.8	4.2	4.9	5.6

Since the conductivity shows gradual increase with temperature, therefore these perovskites behave like semiconductors. The variation of $\text{Ln} \sigma$ as a function of temperature for all samples are exhibited in Fig. (7). Inspecting this figure and observing such variation of the sample LSCF4673, a single straight line is clearly observed, but such variation shows two straight lines for all other samples, intersected at certain temperature differ from one sample to another. However, it can be supposed that the dc conductivity may be due only to the hopping of electrons between the present transition metal cations (iron and cobalt), as well as the hopping of some positive holes through the present oxygen vacancies.

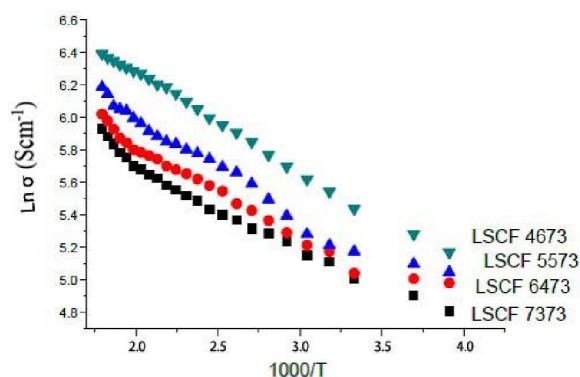


Figure 7. Arrhenius plots for all samples

Since there is some loss of oxygen with increasing temperature, a reduction in the concentration of p-type carriers appeared. And therefore the actual conductivity and the electrical behavior as a function of temperature is somewhat complex. Zeng et al. [40] showed that the thermal induced lattice oxygen loss causes more oxygen deficiency, which may be due to the thermal reduction of Co and Fe cations. Such thermal reduction for transition metals tends to be easier with the increase of La doping [41]. This may explain the reason for the different behaviors at higher temperature range. The variation of the dc conductivity as a function of La content at different fixed temperatures is shown in Fig. (8). It can be observed that the electrical conductivity decreases with the increase of lanthanum, in the whole measured temperature range. The continuous loss of lattice oxygen upon heating can lead to the increase of oxygen vacancies concentration, which can enhance the ionic conductivity.

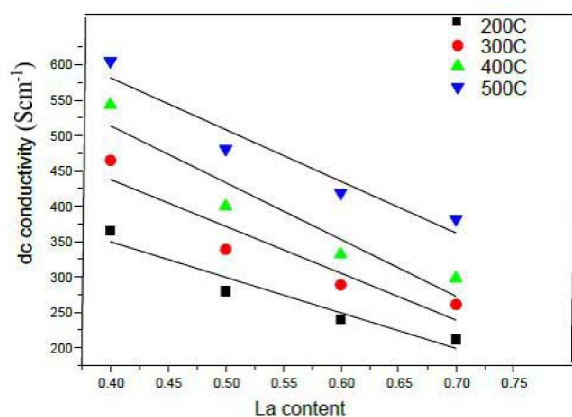


Figure 8. Dc conductivity with La content at different fixed temperatures

3.5 Magnetic Characterization

The vibrating sample magnetometer (VSM) was applied here to investigate the magnetic properties of the studied perovskite samples. The magnetic field was between $\pm 20,000$ Gauss, applied perpendicular to the samples, and the obtained hysteresis loops are presented in Fig. (9). The obtained magnetic parameters (saturation magnetization (M_s), remnant magnetization (M_r) and the coercivity (H_{ci})) are calculated from the measured loops and they are then exhibited in Table (4).

Table 4. The obtained magnetic constants (M_s , M_r and H_{ci}) for all samples

La content	M_s (emu/g)	M_r (emu/g)	H_{ci} (G)
0.4	3.8342	0.63	684.87
0.5	2.5634	0.54	734.98
0.6	1.8642	0.35	815.35
0.7	1.5432	0.21	1587.35

It is seen from this table that M_s and M_r exhibit decreasing trend while H_{ci} shows gradual increase, with the gradual increase of La content. The variation of M_s with La content can be seen in Fig. (10). The observed decrease of both M_s & M_r with La content may be due to the decrease in the canting angle as well as the random distribution of some ortho-ferrite particles through the matrices of the prepared perovskites. This in turn may be due to the substitution of larger strontium ion by smaller lanthanum ion, which in turn may lead to the formation of an inhomogeneous distribution of spin clusters through the perovskite matrices.

On the other hand, the obtained coercivity (H_{ci}) values indicated that all LSCF samples exhibit soft ferromagnetic behavior [42, 43].

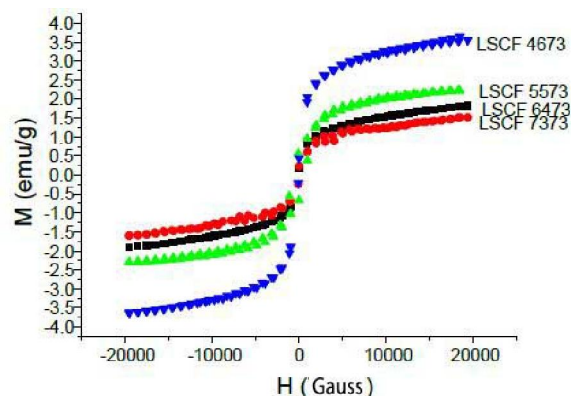


Figure 9. RT (M-H) Hysteresis loops for all samples

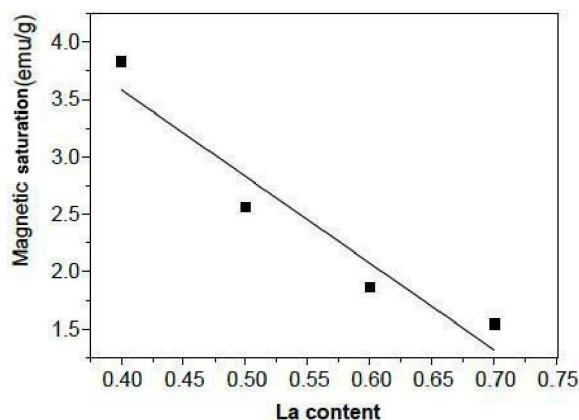


Figure 10. The variation of M_s with La content

3.6. Optical Properties

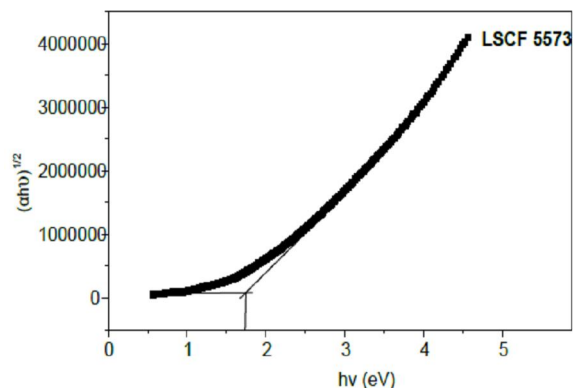


Figure 11. Tauc plot of LSCF5573 perovskite samples as a representative curve

The study of the fundamental absorption edge in the UV-VIS region represents an interesting method for optical transitions and electronic band structure in crystalline and non-crystalline materials. It can be used for the estimation of the optical band gap energies of materials. However, Fig. (11) shows the relation between the photon energy ($h\nu$ eV) and $(\alpha h\nu)^{1/2}$ in eV, for the sample nominated LSCF 5573,

as representative curve, where such plot is usually known as Tauc plot [44].

The calculated band gap values for the studied perovskites are exhibited in Fig. (12) as a function of La content. It appeared that, as La content has gradually increased, the optical band gap energy decreased gradually. This may be due to the increase in the crystallite size and the created oxygen vacancies.

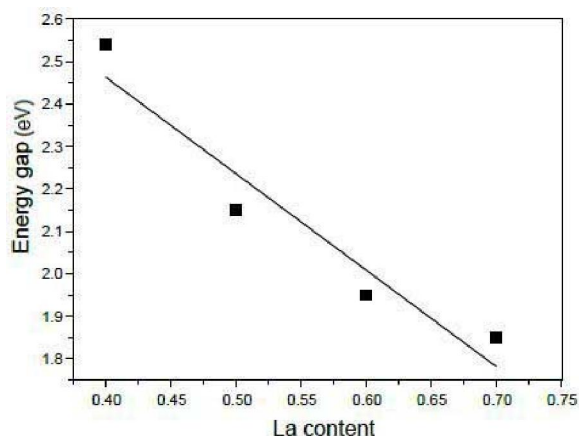


Figure 12. The relation between the optical band gap energy and La content

4. Conclusion

Some $\text{La}_x\text{Sr}_{1-x}\text{Co}_{0.7}\text{Fe}_{0.3}\text{O}_3$ (where $0.4 \leq x \leq 0.7$) perovskite samples have been prepared by the sol-gel method. The calcination temperature was 1000°C , and the duration was 24 h. The distorted rhombohedral crystal structure with very little unreacted CoO for all samples, was characterized by XRD analysis. TEM images show that particles are nano-sized, which is in complete agreement with the values calculated from Scherrer formula (XRD data). The conductivity increased with increasing temperature and controlled by the small polaron hopping model with charge transfer being thermally activated and all samples behave like semiconductors. M_s and M_r are found to decrease uninterruptedly with increasing La doping. The electrical band gap energies increased while the optical band gap energies decreased with increasing La content, accordingly, it is supposed that, the photo-reactivity decreased by increasing La content.

Corresponding Author:

Mohammed G. Ismaeil
Physics Department
Faculty of Science
Aswan Univ., Aswan, Egypt
E-mail: elomdaa_76@yahoo.com

References

1. K. Alex Muller and Tom W Kool, "Properties of perovskites and Other Oxides", World Scientific Publishers, (1986)
2. M.B. Salamon, and M. Jaime, *Rev. Mod. Phys.*, 73 (2001) 583.
3. A. Esquirol, N.P. Brandon, J.A. Kilner, and M. Mogensen, *J. Electrochem. Soc.*, 151 (2004) 1847.
4. A. Petric, P. Huang, and F. Tietz, *Solid State Ionics*, 135 (2000) 719.
5. E. Maguire, B. Gharbage, F.M.B. Marques, and J.A. Labrincha, *Solid State Ionics*, 127 (2000) 329.
6. N.Q. Minh, *J. Am. Ceram. Soc.*, 76 (1993) 563.
7. A. Boudghene Stambouli, and E. Traversa, *Renew Sustain. Energy Rev.*, 6 (2002) 433.
8. E. Ivers-Tiffée, A. Weber and D. Herbstritt, *J. Eur. Ceram. Soc.*, 21 (2001) 1805.
9. H. J. Hwang, J. W. Moon, S. Lee, and E.A. Lee, *J. Power Sources*, 145 (2005) 243.
10. Y.J. Leng, S.H. Chan, S.P. Jiang, and K.A. Khor, *Solid State Ionics*, 170 (2004) 9.
11. Q.L. Liu, K.A. Khor, and S.H. Chan, *J. Power Sources*, 161 (2006) 123.
12. J. Yan, H. Matsumoto, M. Enoki, and T. Ishihara, *Electrochem. Solid-State Lett.*, 8 (2005) 389.
13. S.B. Adler, J.A. Lane, and B.C.H. Steele, *J. Electrochem. Soc.*, 143 (1996) 3554.
14. J.W. Stevenson, T.R. Armstrong, R.D. Carneim, L.R. Pederson and W.J. Weber, *J. Electrochem. Soc.*, 143 (1996) 2722.
15. J. Mizusaki, T. Sasamoto, W.R. Cannon, and H.K. Bowen, *J. Am. Ceram. Soc.*, 66 (1983) 247.
16. J. Mizusaki, M. Yoshihiro, S. Yamauchi, and K. Fueki, *J. Solid State Chem.*, 58 (1985) 257.
17. E. Bucher, and W. Sitte, *Solid State Ionics*, 173 (2004) 23.
18. M. Sogaard, P.V. Hendriksen, and M. Mogensen, *J. Solid State Chem.*, 180 (2007) 1489.
19. V.V. Kharton, A.V. Kovalevsky, M.V. Patrakeev, E.V. Tsipis, A.P. Viskup, V.A. Kolotygin, A.A. Yaremchenko, A.L. Shaula, E.A. Kiselev, and J.C. Waerenborgh, *Chem. Mater.*, 20 (2008) 6457.
20. M.V. Patrakeev, I.A. Leonidov, V.L. Kozhevnikov and K.R. Poeppelmeier, *J. Solid State Chem.*, 178 (2005) 921.
21. M.V. Patrakeev, J.A. Bahteeva, E.B. Mitberg, I.A. Leonidov, V.L. Kozhevnikov, and K.R. Poeppelmeier, *J. Solid State Chem.*, 172 (2003) 219.

22. E.V. Bongio, H. Black, F.C. Raszewski, D. Edwards, C.J. McConville, and V.R.W. Amarakoon, *J. Electroceram.*, 14 (2005) 193.
23. J.E. Ten Elshof, H.J.M. Bouwmeester, and H. Verweij, *Solid State Ionics*, 81 (1995) 97.
24. F. Bidrawn, S. Lee, J.M. Vohs and R.J. Gorte, *J. Electrochem. Soc.*, 155 (2008) 660.
25. S.P. Simner, J.P. Shelton, M.D. Anderson, and J.W. Stevenson, *Solid State Ionics*, 161(2003) 11.
26. A.M. Amesti, A. Larranaga, L.M. R. Martínez, A.T. Aguayoa, J. L. Pizarroa, M.L. No, A. Laresgoiti, and M.I. Arriortua, *J. Power Sources*, 185 (2008) 401.
27. K.T. Lee, and A. Manthiram, *J. Electrochem. Soc.*, 153 (2006) 794.
28. E. Lust, P. Möller, I. Kivi, G. Nurk, and S. Kallip, *J. Solid State Electrochem.*, 8 (2005) 882.
29. J.M. Serra, V.B. Vert, M. Betz, V.A.C. Haanappel, W.A. Meulenber, and F. Tietz, *J. Electrochem. Soc.*, 155 (2008) 207.
30. K. Kammer, *Solid State Ionics*, 177 (2006) 1047.
31. J.H. Piao, K.N. Sun, N.Q. Zhang, X.B. Chen, S. Xu, and D.R. Zhou, *J. Power Sources*, 172 (2007) 633.
32. A. Ecija, K. Vidal, A. Larrañaga, A. Martínez-Amesti, L. Ortega-San-Martín and M.I. Arriortua, *Solid State Ionics*, 201 (2011) 35.
33. A. G. Mostafa, Ibraheem Othman, I. M. Ashraf and M. G. Ismaeil, *Nature and Science*, 14 (2016) 11.
34. X. Yan, J.Chen, Y. Qi, J. Cheng, and Z. Meng, *J. Eur. Ceram. Soc.*, 30 (2010) 265.
35. M. Zawadzki, and J. Trawczy Nski, *Catalysis Today*, 176 (2011) 449.
36. S. Carter, A. Selcuk, R.J. Chater, J. Kajda, J. A. Kilner and B. C. H. Steele, *Solid State Ionic*, 53-56 (1992) 597.
37. L. W. Tai, M.M. Nasrallah, H.U. Anderson, D.M. Sparlin, and S.R. Sehlin, *Solid State Ionics*, 76 (1995) 259.
38. G.C. Kostogloudis, and C.H. Ftikos, *Solid State Ionics*, 34 (1999) 126.
39. L.W. Tai, M. M. Nasrallah, and H.U. Anderson. *Solid State Chem.*, 118 (1995)117.
40. P. Zeng, R. Ran, Z. Chen, H. Gu, Z. Shao and D. D. Costa, *J. Member. Sci.*, 302 (2007) 17.
41. Z. Shao, G. Xiong, J. Tong, H. Dong, and W. Yang, *Sep. Purif. Technol.*, 25 (2001) 419.
42. L. Jiangong, X. Kau, Y. Qin and H. Haiying, *Phys. Status Solidi*, 191 (2002) 255.
43. A. G. Mostafa, E. K. Abdel-khalek, W.M. Daoush and M. Y. Hassan, *Hyperfine Interact.*, 184 (2008) 167.
44. J. Tauc, *Mater. Res. Bull.*, 5 (1970) 37.

10/6/2017